

Integrin adhesion and force coupling are independently regulated by localized PtdIns(4,5)₂ synthesis

Kyle R Legate¹, Seiichiro Takahashi¹,
Navid Bonakdar², Ben Fabry²,
David Boettiger^{1,3}, Roy Zent⁴ and
Reinhard Fässler^{1,*}

¹Department of Molecular Medicine, Max Planck Institute of Biochemistry, Martinsried, Germany, ²Center for Medical Physics and Technology, Department of Physics, University of Erlangen, Erlangen, Germany, ³Department of Microbiology, University of Pennsylvania, Philadelphia, PA, USA and ⁴Division of Nephrology, Department of Medicine, Vanderbilt Medical Center and Veterans Affairs Hospital, Nashville, TN, USA

The 90-kDa isoform of the lipid kinase PIP kinase Type I γ (PIPKI γ) localizes to focal adhesions (FAs), where it provides a local source of phosphatidylinositol 4,5-bisphosphate (PtdIns(4,5)P₂). Although PtdIns(4,5)P₂ regulates the function of several FA-associated molecules, the role of the FA-specific pool of PtdIns(4,5)P₂ is not known. We report that the genetic ablation of PIPKI γ specifically from FAs results in defective integrin-mediated adhesion and force coupling. Adhesion defects in cells deficient in FA-PtdIns(4,5)P₂ synthesis are corrected within minutes while integrin-actin force coupling remains defective over a longer period. Talin and vinculin, but not kindlin, are less efficiently recruited to new adhesions in these cells. These data demonstrate that the specific depletion of PtdIns(4,5)P₂ from FAs temporally separates integrin-ligand binding from integrin-actin force coupling by regulating talin and vinculin recruitment. Furthermore, it suggests that force coupling relies heavily on locally generated PtdIns(4,5)P₂ rather than bulk membrane PtdIns(4,5)P₂.

The EMBO Journal advance online publication, 16 September 2011; doi:10.1038/emboj.2011.332

Subject Categories: membranes & transport; cell & tissue architecture

Keywords: atomic force microscopy; cell adhesion; focal adhesion; PIP kinase; talin

Introduction

Cell adhesion to extracellular matrix (ECM) is mediated by integrins, which regulate their affinity for ligand (also termed integrin inside-out signalling or integrin activation), cluster and couple the ECM to the actin cytoskeleton (Hynes, 2002).

*Corresponding author. Department of Molecular Medicine, Max Planck Institute of Biochemistry, Am Klopferspitz 18, Martinsried 82152, Germany. Tel.: +49 898 578 2072; Fax: +49 898 578 2422; E-mail: faessler@biochem.mpg.de

Received: 26 February 2011; accepted: 19 August 2011

Integrin-mediated coupling of the ECM to F-actin is important to transduce forces from the cytoskeleton to the extracellular environment and to translate external forces into biochemical signals (Friedland *et al*, 2009; Legate *et al*, 2009). The mechanisms that regulate the divergent signalling properties of integrins are poorly understood. However, it is clear that signalling is controlled by hundreds of different molecules that are recruited to integrin cytoplasmic domains (Zaidel-Bar *et al*, 2007; Legate and Fässler, 2009).

The initiation of integrin-mediated adhesion consists of two main steps. The first is the initial activation of integrins, which enables them to bind ligand. The second is the generation of force on the integrin to reinforce this interaction. $\beta 1$ integrin exhibits catch bond behaviour; that is, the application of force increases the lifetime of the integrin-ligand bond (Kong *et al*, 2009). Since the bond lifetime in the absence of force is quite short (<2 s), reinforcement of the integrin-ligand bond should occur rapidly if it is to persist, and the signal to initiate the application of force should originate from within the focal adhesions (FA).

Two molecules that have a key role in integrin activation and in forming a bridge between integrins and the cytoskeleton are talin and the kindlins, which both bind β -integrin cytoplasmic tails (reviewed in Moser *et al*, 2009). The β -integrin tail binding activity of talin is regulated through interactions with the membrane phospholipid phosphatidylinositol 4,5-bisphosphate (PtdIns(4,5)P₂). PtdIns(4,5)P₂ binds the talin head domain, which disrupts an autoinhibitory interaction between the rod domain and the integrin binding region on the talin head and orients talin on the plasmalemma to permit an interaction with β -integrin tails (Anthis *et al*, 2009; Goult *et al*, 2009, 2010; Saltel *et al*, 2009). These observations led to the suggestion that PtdIns(4,5)P₂ represents a regulatory signal for integrin activation. Kindlins contain *bona fide* PH domains that also bind phosphoinositides (Qu *et al*, 2011), but the functional consequences of lipid binding are unknown.

PtdIns(4,5)P₂ comprises ~2.5% of the plasma membrane phospholipid and is relatively evenly distributed throughout the membrane (Hilgemann, 2007). Therefore, it is thought that targeted synthesis and sequestration of PtdIns(4,5)P₂ dictate its temporal and spatial specificity with respect to function (McLaughlin and Murray, 2005). Most PtdIns(4,5)P₂ within the cell is synthesized by Type I phosphatidylinositol 4-phosphate 5-kinases (PIPKIs), which exist in three isoforms in mammals: PIPKI α , PIPKI β and PIPKI γ (Loijens and Anderson, 1996; Ishihara *et al*, 1996, 1998). PIPKI γ consists of up to five splice variants; the major variants are an 87-kDa molecule (PIPKI γ _i1, also called PIPKI γ 635 or PIPKI γ 87) and a 90-kDa molecule (PIPKI γ _i2, also called PIPKI γ 661 or PIPKI γ 90) (Ishihara *et al*, 1998; Giudici *et al*, 2004; Schill and Anderson, 2009). PIPKI γ _i2 differs from PIPKI γ _i1 by the addition of 26 C-terminal amino acids in mouse (28 in

human) that contain a talin binding site and specifically localizes PIPKI γ _i2 to FAs (Di Paolo *et al*, 2002; Ling *et al*, 2002). PIPKI γ _i2 has been shown to be involved in neutrophil polarization (Lokuta *et al*, 2007; Xu *et al*, 2010) regulating LFA-1-mediated T-cell adhesion (Wernimont *et al*, 2010), and promotes the interaction between the cytoskeleton and the membrane in megakaryocytes (Wang *et al*, 2008). The precise role for PIPKI γ _i2 in regulating FAs in non-haematopoietic cells is not established, but the high accumulation of proteins and concomitant exclusion of lipids from FAs means that the local production of PtdIns(4,5)P₂ is likely required to prevent PtdIns(4,5)P₂ from becoming rate limiting.

Structural analysis revealed that the distal talin-binding sequence of the β -integrin tail and of PIPKI γ _i2 bind the same region on the talin head with nM affinity (Barsukov *et al*, 2003; de Pereda *et al*, 2005). Overexpression of PIPKI γ _i2 or the talin-binding peptide causes defects in cell spreading and FA formation suggestive of an integrin activation defect (Di Paolo *et al*, 2002; Ling *et al*, 2002). Therefore, in addition to providing a localized source of PtdIns(4,5)P₂ at FAs, PIPKI γ _i2 may influence FA dynamics by competing directly with β -integrin tails for talin binding. Such a function for PIPKI γ _i2, however, has never been shown.

Since PtdIns(4,5)P₂ has regulatory functions in many cellular processes, general depletion of PtdIns(4,5)P₂ cannot be used to study specific biological functions. Furthermore, genetic ablation of all PIPKI γ isoforms leads to perinatal or embryonic lethality in mice (Di Paolo *et al*, 2004; Wang *et al*, 2007), and has been linked to defects in endocytosis, phagocytosis, cell-cell adhesion and Ca²⁺ signalling (Wang *et al*, 2004; Bairstow *et al*, 2006; Ling *et al*, 2007; Mao *et al*, 2009; Vasudevan *et al*, 2009). Therefore, to define the role for PIPKI γ _i2 in regulating FAs we selectively ablated PIPKI γ _i2 from FAs by deleting the exon encoding the FA targeting signal. This approach provided a unique opportunity to examine the role of a specific pool of PtdIns(4,5)P₂ on integrin function. As predicted, the consequences of disrupting localized PtdIns(4,5)P₂ synthesis resulted in small and transient defects in integrin-mediated cell adhesion and force coupling due to compensation by the bulk membrane diffusion of PtdIns(4,5)P₂. It also demonstrated that talin and

vinculin are less efficiently recruited to new adhesions in the absence of FA-localized PtdIns(4,5)P₂. Thus, in addition to demonstrating the significant role of localized PtdIns(4,5)P₂ in integrin function, this study emphasizes the importance of performing sophisticated sensitive measurements to define subtle alterations in cell function.

Results

Generation of PIPKI γ _i2-deficient fibroblasts

To obtain cells in which PIPKI γ is excluded from FAs, embryonic stem (ES) cells were generated, in which the exon encoding the talin-binding sequence of PIPKI γ (exon 17) was flanked by loxP sites (Supplementary Figure S1). The mutant ES cells were used to establish a mouse strain in which the frt-flanked neo cassette was removed with a transgenic line expressing a deleter flipase. Subsequent Cre-mediated deletion of exon 17 produced mice expressing only the talin binding-deficient PIPKI γ _i1 whose phenotype is currently being analysed and will be described elsewhere. Mixed mouse embryonic fibroblasts (MEFs) and fibroblasts cloned from the kidney of a mouse carrying two floxed exon 17 alleles were generated and exon 17 was deleted *in vitro* using transient adenoviral Cre transduction. The phenotype of the MEFs and the cloned knockout kidney-derived fibroblasts (PIPKI γ Δ E17, hereafter referred to as Δ E17 cells) was compared with parental floxed cells (referred to as WT cells) to avoid differences that could arise from using cells of different origins. Ablation of exon 17 led to the same defects in MEFs and cloned kidney fibroblasts; we display results from the latter cell lines throughout the manuscript, and present confirmation of some of the results in primary MEFs in the supplement.

Western blot analysis revealed that the predominant PIPKI γ splice variant expressed in fibroblasts was PIPKI γ _i1, which lacks the talin-binding sequence. PIPKI γ _i2 was also expressed, albeit at lower levels in wild-type (WT) cells (Figure 1A), and could be easily detected following enrichment of FA proteins using fibronectin (FN)-coated beads (Figure 1B). Although our antiserum did not work efficiently in immunostaining we confirmed prior

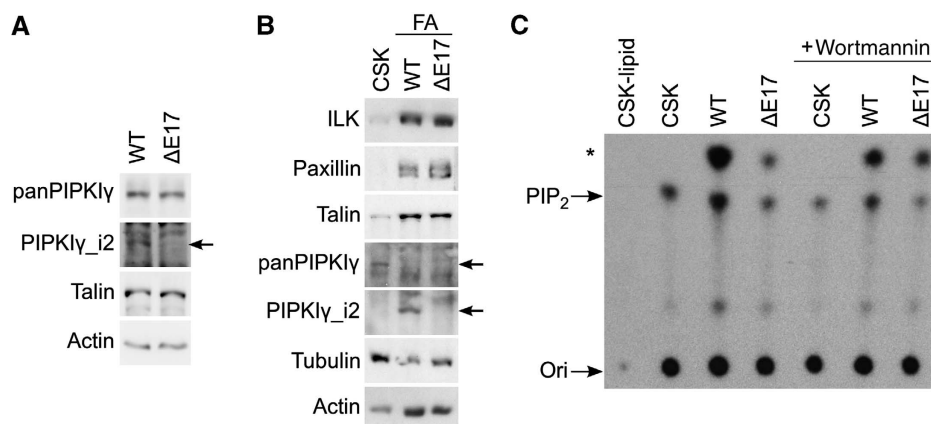


Figure 1 PIPKI γ _i2 is the primary PtdIns(4,5)P₂-generating enzyme at FAs. (A) Western blot analysis of fibroblast protein lysates from WT and Δ E17 cells. In all, 50 μ g of lysate was loaded to detect PIPKI γ _i2, 20 μ g of lysate was loaded to detect PIPKI γ and talin, and 5 μ g of lysate was loaded to detect actin. (B) Western blot analysis of cytoskeletal extract (CSK) from WT cells, and enriched FA fractions from WT and Δ E17 cells. (C) Kinase assays using equal protein amounts of CSK from WT cells, and enriched FA fractions from WT and Δ E17 cells, analysed by thin layer chromatography. The migration positions of PtdIns(4,5)P₂ (PIP₂) and an unidentified lipid contaminant from the FA preparation (asterisk) are identified. Ori, origin. Figure source data can be found in Supplementary data.

reports demonstrating that PIP1K1 γ _i2 localizes specifically to FAs (Di Paolo *et al*, 2002; Ling *et al*, 2002; Supplementary Figure S2).

FA-enriched fractions were isolated from fibroblasts to determine whether they could support the synthesis of PtdIns(4,5)P₂ *in vitro*. The adhesion molecules talin, paxillin and ILK were enriched in FAs and present in comparable amounts in WT and Δ E17 protein isolates (Figure 1B). PIP1K1 γ _i2 was detected in isolates from WT cells, but not in Δ E17 isolates (Figure 1B). The ability of FA fractions to support PtdIns(4,5)P₂ synthesis was tested by using equivalent amounts of FA isolates in *in vitro* kinase assays (Figure 1C). WT FA isolates readily converted phosphatidylinositol 4-phosphate (PtdIns(4)P) to a bisphosphorylated form. In contrast, FA isolates from Δ E17 cells showed decreased phosphorylation of PtdIns(4)P. Inhibition of PI 3-kinase with wortmannin caused only a modest reduction in PtdIns(4)P phosphorylation, indicating that it was not the dominant lipid kinase activity in the assay. The residual phosphorylation in these extracts was probably due to traces of other PIP kinase isoforms.

These data confirm that mouse fibroblasts express both PIP1K1 γ _i1 and PIP1K1 γ _i2, and demonstrate that it is feasible to remove PIP1K1 γ from FAs by deleting the PIP1K1 γ _i2-specific exon 17.

FA-specific PtdIns(4,5)P₂ increases the rate of talin accumulation in FAs

To investigate how early stages of adhesion formation are altered in the absence of local PtdIns(4,5)P₂ synthesis, we monitored the incorporation rates of specific molecules into FAs using TIRF microscopy (Figure 2A–E). Talin1, vinculin and kindlin 2 were selected for this analysis because talin and vinculin bind PtdIns(4,5)P₂ (Goksoy *et al*, 2008; Palmer *et al*, 2009), and kindlin 2 contains a PH domain and also binds phosphoinositides (Qu *et al*, 2011). Paxillin incorporation was monitored as it is believed not to be influenced by PtdIns(4,5)P₂. Each protein was tagged with GFP and incorporation rates were calculated by monitoring the increase in fluorescence in individual new FAs over time (Figure 2A). The incorporation rates of each of these proteins in WT cells were similar to a previously reported rate of paxillin accumulation into FAs in fibroblasts (Doan and Huttenlocher, 2007). In the absence of local PtdIns(4,5)P₂ synthesis, the incorporation rate of talin1 into new FAs was diminished by half (Figure 2A and B; Supplementary Figure S3A; Supplementary Movie 1). The incorporation rate of vinculin was also decreased by half as expected for talin-dependent recruitment of vinculin to FAs (Critchley, 2004; Zhang *et al*, 2008; Figure 2C). In contrast, recruitment of kindlin 2 and paxillin to new FAs was insensitive to PIP1K1 γ _i2 (Figure 2D and E; Supplementary Figure S4A). The independence of kindlin 2 recruitment and increased local PtdIns(4,5)P₂ raises the issue of why it was not affected despite the presence of a potential PtdIns(4,5)P₂ binding domain. To explore the reason for this insensitivity, we used a vesicle sedimentation assay to determine the phosphoinositide binding profile of kindlin 2 in the context of a lipid bilayer. We found that both kindlin 2 and the talin head domain cosedimented with vesicles containing either PtdIns(4,5)P₂ or PtdIns(3,4,5)P₃, although kindlin 2 sedimented more efficiently with PtdIns(3,4,5)P₃ (Supplementary Figure S4B). Therefore,

although kindlin 2 bound to PtdIns(4,5)P₂ *in vitro*, this lipid was not a recruitment signal for kindlin 2 *in vivo*.

To examine the possibility of a kinase-independent role for PIP1K1 γ _i2 in talin trafficking, we monitored talin recruitment to new adhesions in Δ E17 cells expressing kinase-dead PIP1K1 γ _i2 (PIP1K1 γ KD; Figure 2F). PIP1K1 γ _i2 KD failed to increase the rate of talin recruitment, thus eliminating the possibility that PIP1K1 γ _i2 functions as an adapter to direct talin to FAs. The recruitment was slightly decreased, probably owing to competition between PIP1K1 γ _i2 and the β -integrin tail for binding to the talin head, but the low expression level of PIP1K1 γ KD rendered the effect of competition insignificant. In contrast, expression of WT PIP1K1 γ _i2 in Δ E17 cells rescued the recruitment of talin to FAs. Therefore, the kinase activity of PIP1K1 γ _i2 is essential for the normal recruitment rate of talin to new FAs, and the advantage imparted by local synthesis of PtdIns(4,5)P₂ more than compensates for any competition between PIP1K1 γ _i2 and β -integrin at the expression level achieved in this assay.

To dissect which of the talin-mediated PtdIns(4,5)P₂-dependent functions are affected by the loss of localized PtdIns(4,5)P₂ production, we created mutations within talin either to disrupt the autoinhibitory interaction or to disrupt the orientation of the talin head on the plasma membrane. The ‘unclasp’ mutations K318A/K320A within the F3 domain, or the E1770K mutation within the talin rod did not change the incorporation rate into new adhesions compared with WT talin, indicating that release of talin autoinhibition was not the rate-limiting step for incorporation into FAs (Figure 2G). To examine whether orientation of talin on the plasma membrane is disrupted, we made a mutation within a basic ridge of the talin F2 domain (K274E) which was shown to reduce the interaction of talin with acidic phospholipids (Anthis *et al*, 2009; Saltel *et al*, 2009). This mutation reduced the incorporation rate of talin into new FAs in WT cells to a similar extent as for WT talin in Δ E17 cells (Figure 2H). Taken together, these data show that PtdIns(4,5)P₂ synthesized by PIP1K1 γ _i2 facilitates talin recruitment to FAs through an interaction between PtdIns(4,5)P₂ and the basic ridge on the talin F2 subdomain, rather than through relieving the autoinhibitory interaction.

FA-specific PtdIns(4,5)P₂ is critical for establishing cell adhesion

To obtain an approximate measure of initial adhesion in the presence or absence of local PtdIns(4,5)P₂ synthesis, we conducted a ‘plate-and-wash’ adhesion assay on FN-coated dishes as a function of time (Figure 3A and B). This assay measures the rate that cells attach to a substrate, but does not provide an indication of the number of adhesive bonds or how strongly cells adhere (Boettiger and Wehrle-Haller, 2010). The rate of attachment of Δ E17 cells was significantly decreased compared with WT cells in magnesium-containing adhesion buffer (rate constant $0.067 \pm 0.021/\text{min}$ (WT) versus $0.036 \pm 0.018/\text{min}$ (Δ E17); Figure 3A); the adhesion was integrin-specific as incubation with 100 μM cilengitide, a concentration that blocks both β 1- and β 3-integrins (Frank *et al*, 2010), largely abolished binding to the FN-coated dish (Figure 3A). When manganese was used in place of magnesium to bypass inside-out signalling there was no difference in the rate constants for cell attachment ($0.102 \pm 0.044/\text{min}$ for WT versus $0.108 \pm 0.057/\text{min}$ for Δ E17; Figure 3B). Thus,

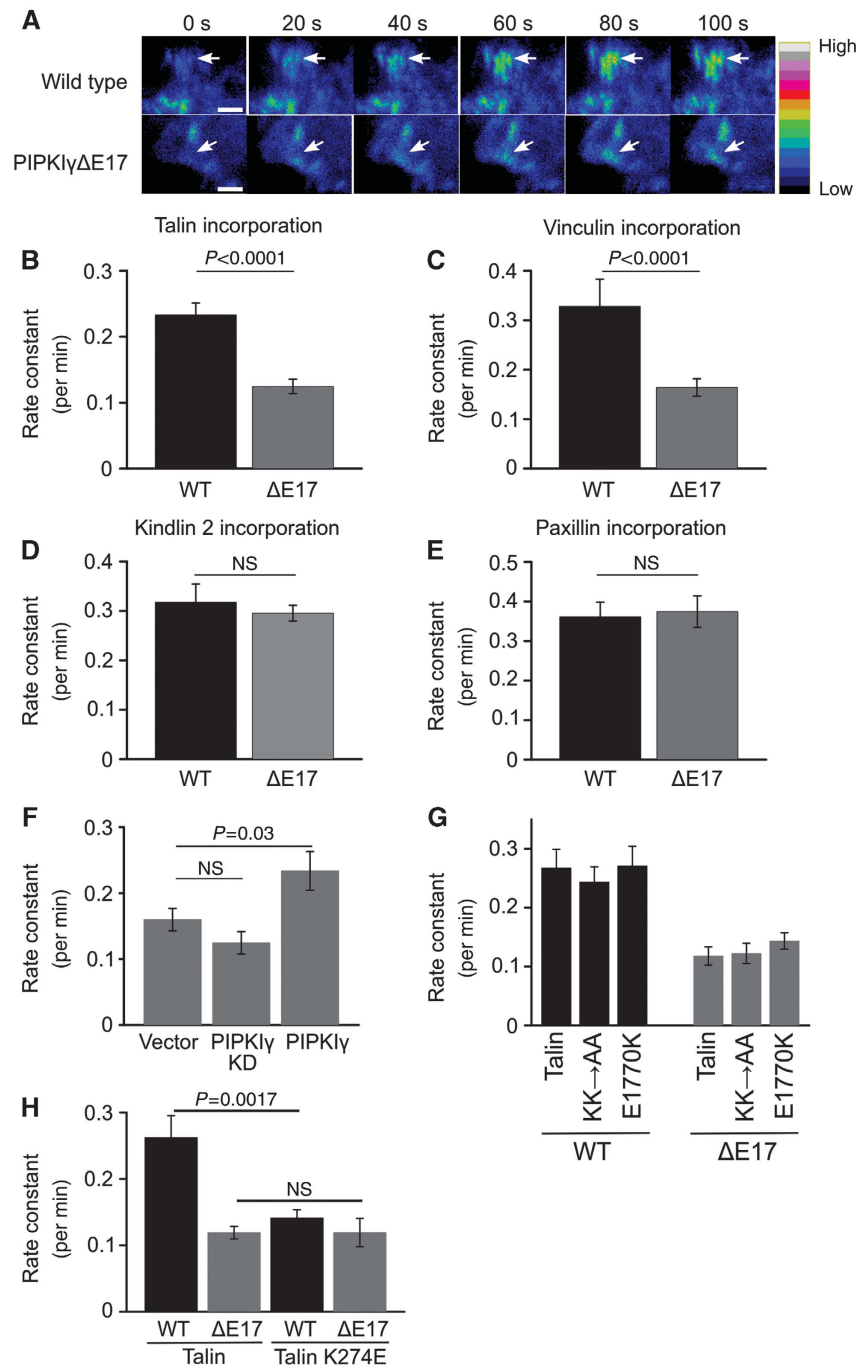


Figure 2 Talin and vinculin recruitment to new FAs is impaired in PIPKI γ ΔE17 fibroblasts. (A) TIRF time-lapse images were collected from the leading edge of GFP-talin-expressing WT or ΔE17 fibroblasts. The incorporation of talin into new adhesions (arrows) was monitored by quantifying the rate of increase in GFP epifluorescence. Heatmaps of pixel intensities from a representative example are shown. (B–E) Rate constants of incorporation were determined from the linear phase of GFP epifluorescence increase in cells expressing GFP-tagged (B) talin ($n=11$ WT, 9 ΔE17), (C) vinculin ($n=7$ WT, 7 ΔE17), (D) kindlin2 ($n=6$ WT, 7 ΔE17) and (E) paxillin ($n=6$ WT, 6 ΔE17). (F) Talin incorporation rate was calculated for ΔE17 cells expressing GFP (vector; 4 cells), kinase-dead GFP-PIPKI γ _i2 (PIPKI γ KD; 7 cells) or wild-type GFP-PIPKI γ _i2 (PIPKI γ ; 6 cells). (G) The incorporation rates of the talin ‘unclasping’ mutants K318A/K320A (KK→AA) and E1770K were calculated in WT cells ($n=6$ KK→AA, 8 E1770K) and ΔE17 cells ($n=9$ KK→AA, 6 E1770K). (H) The incorporation rate of talinK274E was compared with the incorporation rate of WT talin in WT ($n=6$ WT, 5 K274E) and ΔE17 cells ($n=5$ WT, 5 K274E). All data are mean \pm s.e.m. Mann-Whitney tests were used to establish statistical significance in (B–H); NS = not significant. Scale bar in (A) = 1 μ m.

PtdIns(4,5)P₂ synthesized by PIPKI γ _i2 contributes to the initial attachment of cells to FN. Since diffusion would supply PtdIns(4,5)P₂ synthesized by other PIPKI isoforms, we used single-cell atomic force microscopy (AFM) to measure formation of adhesive bonds during the first seconds of cell-

substrate contact. Cells attached to the AFM cantilever were brought into contact with a FN-coated surface for 10–30 s and then the cantilever was retracted from the surface, generating a detachment force curve. Detachment force was calculated as the maximum deflection of the AFM cantilever from the

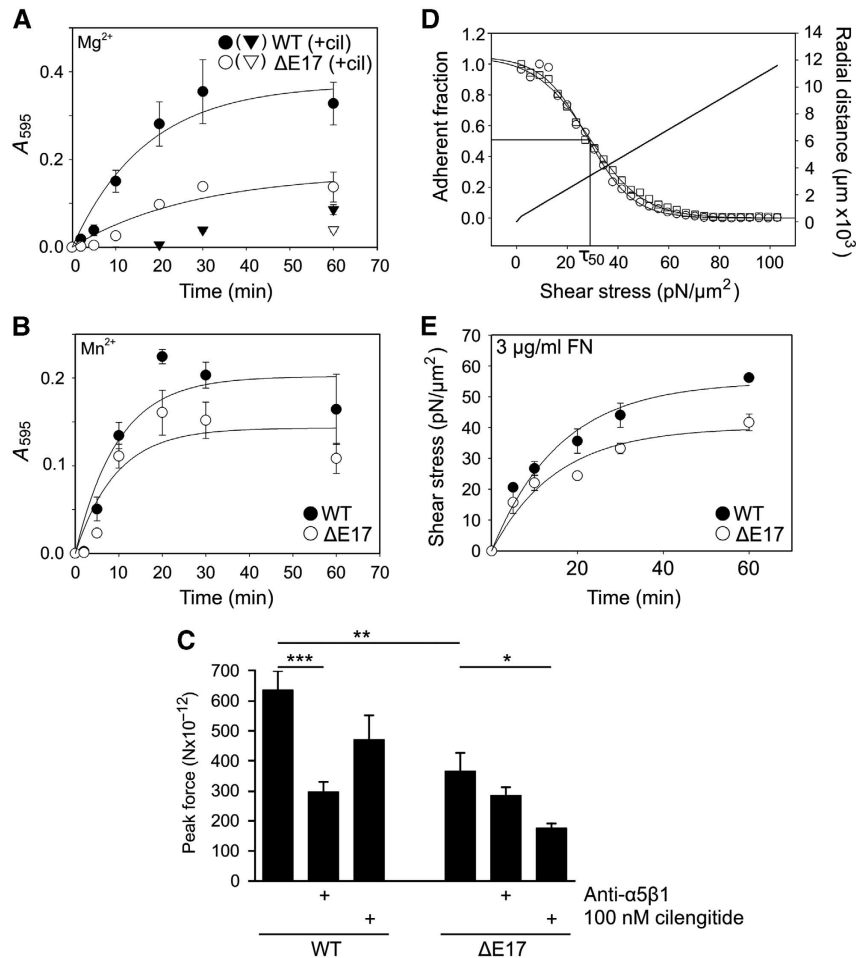


Figure 3 Initial adhesion is reduced in PIPKI Δ E17 fibroblasts but rate of bond accumulation is unchanged. (A) Plate-and-wash assay performed with WT (filled circles) and Δ E17 fibroblasts (open circles) plated onto 2 μ g/ml FN-coated plastic in the presence of 1 mM Mg^{2+} . Experiments including 100 μ M cilengitide are depicted by triangles. Data are mean \pm s.e.m. for three independent experiments. Exponential rise-to-max best-fit lines were used to determine kinetic parameters. (B) Plate-and-wash assay as in (A) but performed in the presence of 1 mM Mn^{2+} . (C) Cells were attached to a tipless cantilever and brought into contact with a 2 μ g/ml FN-coated surface for 30 s. To probe for the contribution of $\alpha 5\beta 1$ and $\alpha \nu\beta 3$ to adhesion, an $\alpha 5\beta 1$ function blocking antibody or 100 nM cilengitide was used, respectively. Data are mean \pm s.e.m. of 10 cells per condition. (D, E) A spinning disc assay was used to analyse relative numbers of adhesive bonds. (D) Typical data obtained from this assay following a 30-min incubation and 5-min spin. Shear stress increases linearly as a function of the radial distance from the centre (depicted by the diagonal line). The profile of cell detachment follows a sigmoid curve (WT cells = open circles; Δ E17 cells = open squares). The τ_{50} value, or the mean shear stress required for cell detachment, is shown. (E) Spinning disc data for WT cells (closed circles) and Δ E17 cells (open circles) plated onto 3 μ g/ml FN-coated coverslips for the indicated time periods. Data are mean \pm s.e.m. for three independent experiments, conducted in duplicate. Exponential rise to max curves were used to determine kinetic parameters. * $P < 0.05$; ** $P < 0.005$; *** $P < 0.0005$.

baseline (Supplementary Figure S5A). To distinguish between integrin-dependent and integrin-independent adhesion, we blocked integrin function by incubating cells with a linear RGD peptide (Supplementary Figure S5A and B). The difference between the force required to detach cells in the presence and absence of the peptide corresponds to integrin-dependent adhesion. At both time points tested, the integrin-dependent adhesion arising from Δ E17 cells was reduced compared with WT cells, indicating that the localized production of PtdIns(4,5) P_2 at adhesion sites was important for the initial interaction of integrins with FN (Supplementary Figure S5B). As both $\alpha 5\beta 1$ - and $\alpha \nu\beta 3$ -integrins can contribute to FN binding, we used specific integrin blockers to test whether PIPKI γ i2 activity affects the function of $\beta 1$ - and $\beta 3$ -integrins differently (Figure 3C). Antibody-mediated blockade of $\alpha 5\beta 1$ activity significantly reduced the detach-

ment force of WT cells, whereas Δ E17 cells, which had markedly reduced detachment force compared with WT cells in the absence of inhibitors, were not significantly affected by $\alpha 5\beta 1$ blockade. The addition of 100 nM cilengitide, a low concentration that specifically blocks $\beta 3$ -integrins (Frank *et al*, 2010), reduced the detachment force of both cell lines by ~ 180 pN; furthermore, a plate-and-wash assay using 5 μ g/ml vitronectin as an $\alpha \nu\beta 3$ -specific ligand showed comparable binding between the cell lines (Supplementary Figure S6; rate constant 0.034 ± 0.018 for WT and 0.029 ± 0.021 for Δ E17), indicating that the adhesive contribution of $\beta 3$ -integrins is unchanged in the absence of PIPKI γ i2. Therefore, reduced PtdIns(4,5) P_2 at FAs reduced $\alpha 5\beta 1$ -dependent cell adhesion.

To assess the effect of PIPKI γ i2 on the increase in adhesive $\alpha 5\beta 1$ bonds, we employed a spinning disc adhesion

assay, in which the force required for cell detachment is proportional to the number of adhesive integrin–FN bonds (García *et al*, 1998; Boettiger, 2007). In this assay, cells are uniformly plated onto FN-coated coverslips and subjected to a linear hydrodynamic shear stress gradient in a buffer-filled chamber. Cells at the centre of the disc are exposed to negligible shear, whereas shear force increases linearly with distance from the centre (Figure 3D, diagonal line). The cell detachment profile fits a sigmoid curve from which the mean shear stress required to detach a cell (τ_{50}) is calculated (Figure 3D). This value is proportional to the number of adhesive bonds (in this case bonds between cell surface integrin and FN) (García *et al*, 1998; Shi and Boettiger, 2003; Boettiger, 2007). After 5 min of adhesion, few $\Delta E17$ cells could be observed on the coverslip (Supplementary Figure S7A) supporting the plate-and-wash and AFM data, demonstrating that local PtdIns(4,5) P_2 synthesis is important for the initial attachment event. Once the cells had adhered the rate of increase in the number of adhesive integrin–ligand bonds was similar for WT and $\Delta E17$ (rate constant for 3 $\mu\text{g}/\text{ml}$ FN coating $0.062 \pm 0.013/\text{min}$ for WT versus $0.066 \pm 0.018/\text{min}$ for $\Delta E17$; Figure 3E), although the number of $\Delta E17$ cells adhered to the disc remained lower than WT (Supplementary Figure S7A). A higher FN coating density (5 $\mu\text{g}/\text{ml}$) rendered differences between WT and $\Delta E17$ cells insignificant (Supplementary Figure S7B and C). Consistent with an insensitivity of $\beta 3$ -integrins to PIPKI γ_{i2} loss, adhesion to vitronectin (2 $\mu\text{g}/\text{ml}$) resulted in the same mean shear force required to detach both cell lines (Supplementary Figure S7D). However, low numbers of cells counted on the coverslip at early times prevented rate constants from being calculated (Supplementary Figure S7E). Incubation with 100 μM cilengitide greatly reduced the number of cells that adhered to the coverslip (Supplementary Figure S7F). Thus, local PtdIns(4,5) P_2 affected the initial attachment as suggested above but had little or no effect on the rate of formation of $\alpha 5\beta 1$ –FN bonds once the cells attached.

Formation of new FAs in newly attached cells

To monitor the appearance of FAs in adherent cells over time, GFP–talin-transfected cells were plated onto FN for discrete time intervals and immunostained for paxillin (Figure 4A–C). Peripheral adhesions containing both paxillin and talin were well formed in WT cells after 20 min, whereas $\Delta E17$ cells showed a punctate localization of paxillin throughout the basal cell membrane that was relatively deficient in talin (Figure 4A). Between the 20- and 40-min time points the peripheral adhesion structures matured into elongated FAs in WT cells and were fully matured after 60 min. In contrast, adhesion maturation appeared to be delayed in $\Delta E17$ cells, with talin colocalization with paxillin apparent after 40 min (Figure 4A). Quantifying the cell area occupied by adhesion structures revealed a significant reduction in the paxillin-positive area in $\Delta E17$ cells after 1 h of plating (Figure 4B). Phalloidin staining indicated that actin fibrils were able to anchor to FAs in both cell lines (Supplementary Figure S8). Morphometric analysis of FA length in cells plated for 1 h revealed that while 30% of WT adhesions were $> 3 \mu\text{m}$ in length, only 10% of $\Delta E17$ adhesions were $> 3 \mu\text{m}$ long (Figure 4C), supporting delayed maturation of $\Delta E17$ FAs.

Next, we plated cells on different concentrations of FN to assess their spreading behaviour. One hour after plating,

$\Delta E17$ cells were significantly less spread than their WT counterparts (Figure 4D and E; Supplementary Figure S3B); this difference was abolished following a longer incubation (Figure 4D), indicating that while $\Delta E17$ cells are impaired at early time points, at steady state they perform as well as WT cells. During 1 h of spreading, $\Delta E17$ cells plated on the lowest density of FN (coated at 2 $\mu\text{g}/\text{ml}$) achieved a two-fold increase in spread area, whereas WT cells increased their area four- to five-fold (Figure 4E); less dramatic differences were observed at higher densities of FN.

Importantly, the adhesion and spreading defects in $\Delta E17$ cells were not due to reduced surface expression levels of FN-binding integrins. FACS analysis showed similar levels of $\alpha 5\beta 1$ and $\alpha v\beta 3$ surface expression (Supplementary Figure S9A). Nor were the differences due to an intrinsic inability of integrins to respond to ligand. Incubation with soluble RGD ligand resulted in similar increases in 9EG7 antibody binding, a reporter for the ‘active’ $\beta 1$ -integrin conformation (Supplementary Figure S9B). One hour after plating, cell staining with the 9EG7 antibody was similar for WT and $\Delta E17$ cells (Supplementary Figure S9C).

Altogether these data indicate that FA-localized PtdIns(4,5) P_2 synthesis facilitates cell adhesion (the binding of integrins) by accelerating the recruitment of talin to new adhesions. PtdIns(4,5) P_2 affects the early stages of cell attachment and FA maturation most profoundly but once cells become stably adherent the accumulation of additional bonds was not reduced by FA-localized PtdIns(4,5) P_2 deficiency.

FA-specific PtdIns(4,5) P_2 is important for development of force generation

Thus far our assays failed to demonstrate that the inside-out function of talin in promoting integrin activation is impaired in the absence of localized PtdIns(4,5) P_2 synthesis. However, adherent $\Delta E17$ cells exhibited a spreading defect despite a normal rate of accumulation of integrin–ligand bonds (as measured by the spinning disc assay). Therefore, FA-specific PtdIns(4,5) P_2 synthesis likely serves additional functions. Since the generation of intracellular force is required for cells to spread we examined the ability of integrins to transduce force in the absence of localized PtdIns(4,5) P_2 synthesis. Previous work has shown that the spinning disc assay measures the total number of bound integrins per cell independently of cytoskeletal tension, but only tensioned integrins can be crosslinked to ligand (Friedland *et al*, 2009). We, therefore, monitored $\beta 1$ -integrin crosslinking to a 5 $\mu\text{g}/\text{ml}$ FN-coated surface as a function of time. During the first 2 h after cell plating, the amount of crosslinked $\beta 1$ -integrin was reduced by half in $\Delta E17$ cells compared with WT cells (Figure 5A, $2.04 \pm 0.11\%$ for WT cells versus $1.11 \pm 0.09\%$ for $\Delta E17$ cells), although spinning disc analysis showed that the total number of bonds was not reduced in the $\Delta E17$ cells at this FN concentration (Supplementary Figure S7B). The reduced proportion of crosslinked $\beta 1$ -integrin indicates a reduction in the number of tensioned integrins (Friedland *et al*, 2009), suggesting that local PtdIns(4,5) P_2 synthesis promotes force coupling of integrins to ligand. The ability of cells to exert force on their environment was also examined by monitoring the contraction of FN-impregnated collagen gels seeded with WT or $\Delta E17$ cells. The data in Figure 5B and C clearly show that $\Delta E17$ cells contracted

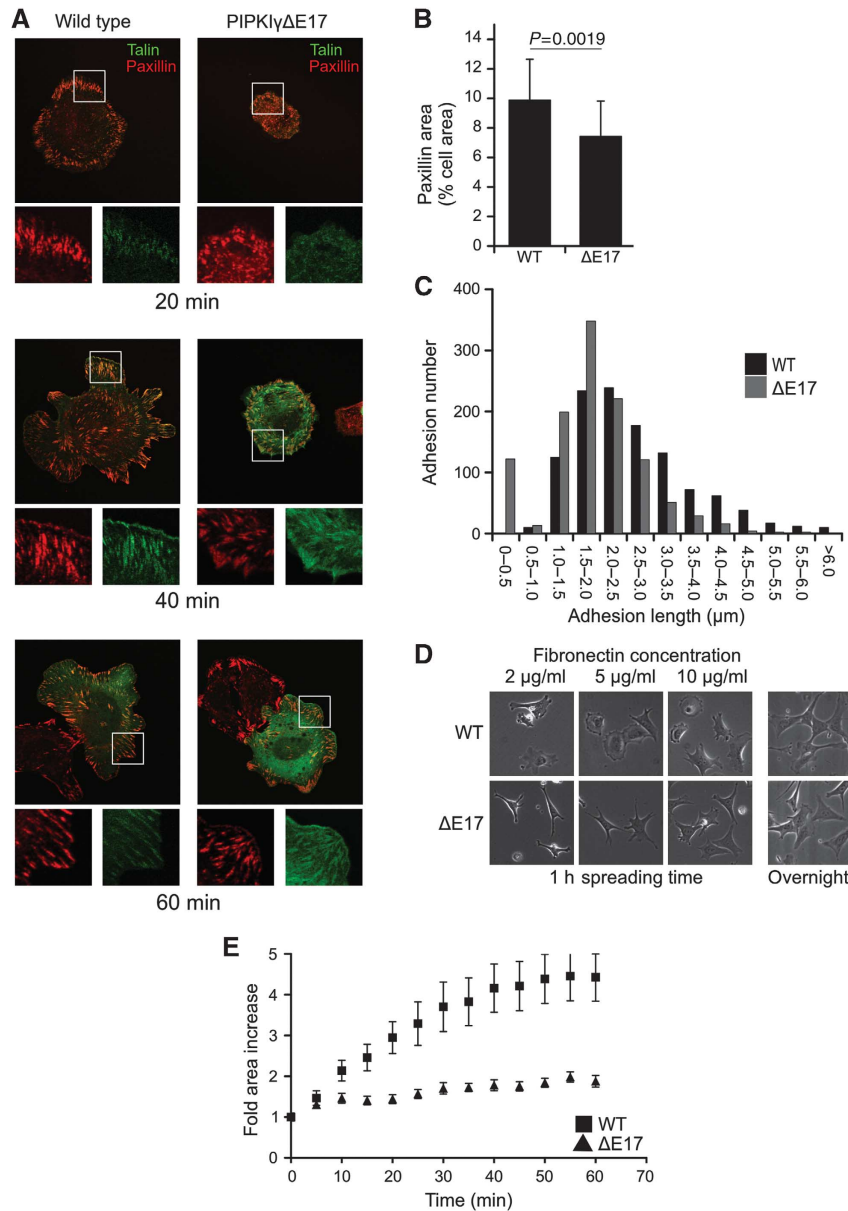


Figure 4 FA formation and cell spreading are delayed in the absence of local PtdIns(4,5)P₂ synthesis. **(A)** Immunofluorescence images of WT and Δ E17 fibroblasts expressing GFP-talin (green) and immunostained for paxillin (red) after 20, 40 or 60 min of spreading on 5 μ g/ml FN-coated glass coverslips. Boxed areas in the upper panels are magnified in the lower panels. **(B)** Quantification of the cell area occupied by FAs in 25 cells of each genotype. Values are mean \pm s.d. A Mann-Whitney test was used to establish statistical significance. **(C)** FA lengths measured from cells immunostained for paxillin were measured and binned into 0.5 μ m increments to obtain a comparative distribution of FA length in WT (black bars, 1128 FAs from 10 cells) and Δ E17 (grey bars 1006 FAs from 10 cells) cells. **(D)** Representative bright field images of WT and Δ E17 fibroblasts plated onto plastic dishes coated with the indicated concentrations of FN for 1 h, or overnight in the absence of serum. **(E)** Temporal analysis of spreading behaviour for the cells plated on 2 μ g/ml fibronectin. Squares = wild type; triangles = Δ E17. Values are mean \pm s.e.m. for 15 cells of each genotype.

the collagen gels less efficiently than WT control cells. Exponential decay curves fit to the data in Figure 5C revealed a four-fold reduction in the rate constant for collagen gel contraction by Δ E17 cells (WT = 0.209 ± 0.027 /h; Δ E17 = 0.052 ± 0.042 /h).

To obtain a direct measure of force, WT and Δ E17 cells were plated onto 5 μ g/ml FN-coated flexible polyacrylamide gels embedded with fluorescent beads ($E = 12.8$ kPa). The elastic strain energy stored in the gel as a result of cell traction was calculated as the product of local deformations of the gel (Figure 5D). When normalized for cell area the strain energy imparted by Δ E17 cells was half of that imparted by WT cells (Figure 5E). In contrast, no differences

were observed in phosphorylation of myosin light chain (MLC) as measured by glycerol-urea PAGE, a proxy measure of activation of myosin contraction (Figure 5F). Therefore, the defect probably lies at the level of the integrin-actin interaction.

The transition between lamellipodium and lamellum (characterized by fast actin retrograde flow and slow actin flow, respectively) is marked by the formation of focal complexes, which capture actin filaments and act as a clutch (Alexandrova *et al*, 2008; Giannone *et al*, 2009). We reasoned that if the integrin-actin clutch is defective in Δ E17 cells the formation of the lamellipodium-lamellum border may be delayed, leading to a wider lamellipodium. Using enhanced

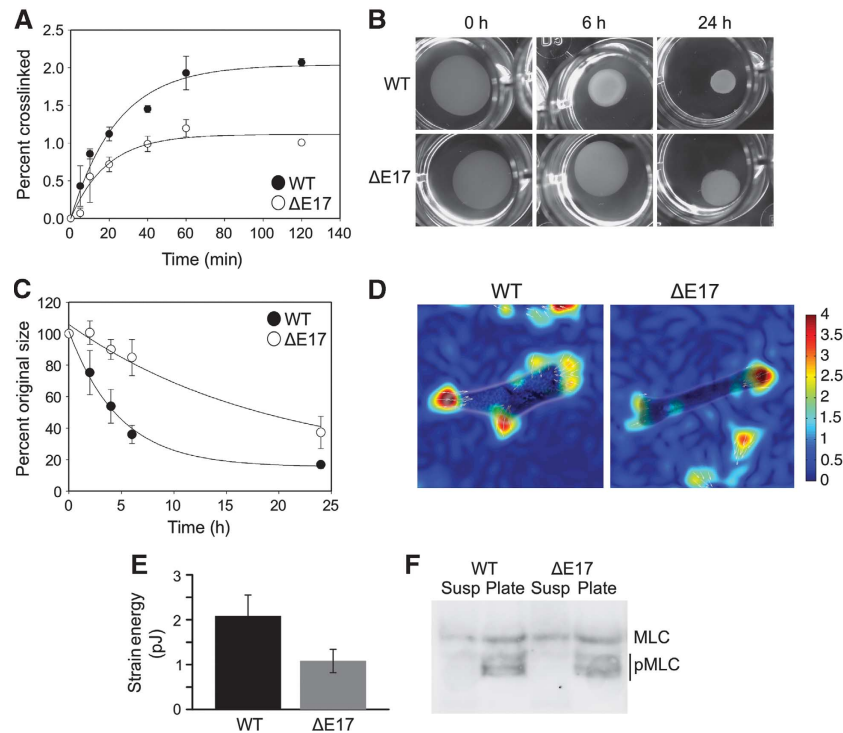


Figure 5 Integrin bond tensoning is reduced in the absence of localized PtdIns(4,5)P₂ synthesis. **(A)** Cells were plated onto 5 μ g/ml FN-coated plastic for the incubated times and integrins were crosslinked with the extracellular crosslinker DTSSP. The amount of crosslinked β 1-integrin from WT (closed circles) and Δ E17 cells (open circles) was quantified from western blots and best-fit curves were fitted to a first order exponential function as described in Materials and Methods. Data are mean \pm s.e.m. for three experiments. **(B, C)** Contraction of collagen gels was used to assess force transduction to the extracellular environment. Plugs of a collagen and FN mixture containing 3×10^5 cells were photographed at defined time intervals. **(B)** A representative experiment and **(C)** the mean \pm s.e.m. of four independent experiments are shown. Exponential decay curves were used to determine kinetic parameters. **(D)** Strain energy heatmaps of wild-type (WT) and Δ E17 cells plated onto FN-coated polyacrylamide supports ($E = 12.8$ kPa). Bright field and traction field images are overlaid to show the position of the cell. **(E)** The product of the strain energy normalized for cell area is presented. **(F)** Cells were plated for 6 h or kept in suspension for 1 h and myosin light chain (MLC) phosphorylation was assessed by glycerol-urea PAGE. The migration positions of MLC and phospho-MLC (pMLC) are indicated. Figure source data can be found in Supplementary data.

phase contrast microscopy to directly observe actin flow within the narrow lamellipodium (Verkhovsky *et al*, 2003; Alexandrova *et al*, 2008; Figure 6A and C; Supplementary Movie 2A and B) we could visualize fast retrograde actin flow that manifested as dark bands in kymographs (Figure 6B and D). The net forward movement of the cell front in the kymographs shows that protrusive lamellipodia were analysed in both WT and Δ E17 cells. By measuring the length and angle of the dark bands, we determined that the velocity of retrograde actin flow was unchanged between WT and Δ E17 cells (Figure 6E); however, the width of the lamellipodium was significantly increased in Δ E17 cells (Figure 6F). This indicates that the actin cytoskeleton was less coupled, and therefore not slowed as efficiently by the integrin clutch. Consistent with this, stable talin-rich adhesions were present at the lamellipodium–lamellum border in WT cells and were excluded from the lamellipodium (Figure 6G), whereas in Δ E17 cells stable adhesions extended beneath the cortactin-rich lamellipodium to the edge of the cell (Figure 6H).

Despite several lines of evidence supporting a force coupling defect in Δ E17 cells, it is interesting to note that migration defects were not apparent in these cells. Both a scratch assay and single-cell tracking assay failed to uncover differences in migration speed (Figure 7A; Supplementary Figures S3C and S10) or persistence (Euclidean distance/accumulated distance; WT = 0.44, Δ E17 = 0.46; Figure 7B)

in two-dimensional culture compared with WT controls. Chemotactic migration towards a gradient of epidermal growth factor (EGF) was likewise not affected at all concentrations tested but migration towards platelet-derived growth factor (PDGF) was abolished in Δ E17 cells (Figure 7C), supporting a role for PIPK1 γ in chemotactic response to certain growth factors (GFs; Sun *et al*, 2007).

Discussion

The assembly and disassembly of FAs and their linkage to the F-actin cytoskeleton are tightly controlled by complex combinations of post-translational modifications including phosphorylation, dephosphorylation, ubiquitination and proteolysis. Additionally, the proximity of the plasma membrane makes it likely that protein–phospholipid interactions also participate in the control of FA function. Several FA molecules including talin and vinculin can bind to the lipid PtdIns(4,5)P₂ and PIPK1 γ , one of several lipid kinase isoforms in the cell that make PtdIns(4,5)P₂, localizes to FAs, raising the possibility that FA-localized PtdIns(4,5)P₂ synthesis has a specific regulatory function within FAs. We sought to understand which aspects of FA function are controlled by PtdIns(4,5)P₂. To avoid a large, global perturbation of PtdIns(4,5)P₂ within the cell, we ablated the FA localization of PIPK1 γ to achieve a small but specific depletion of

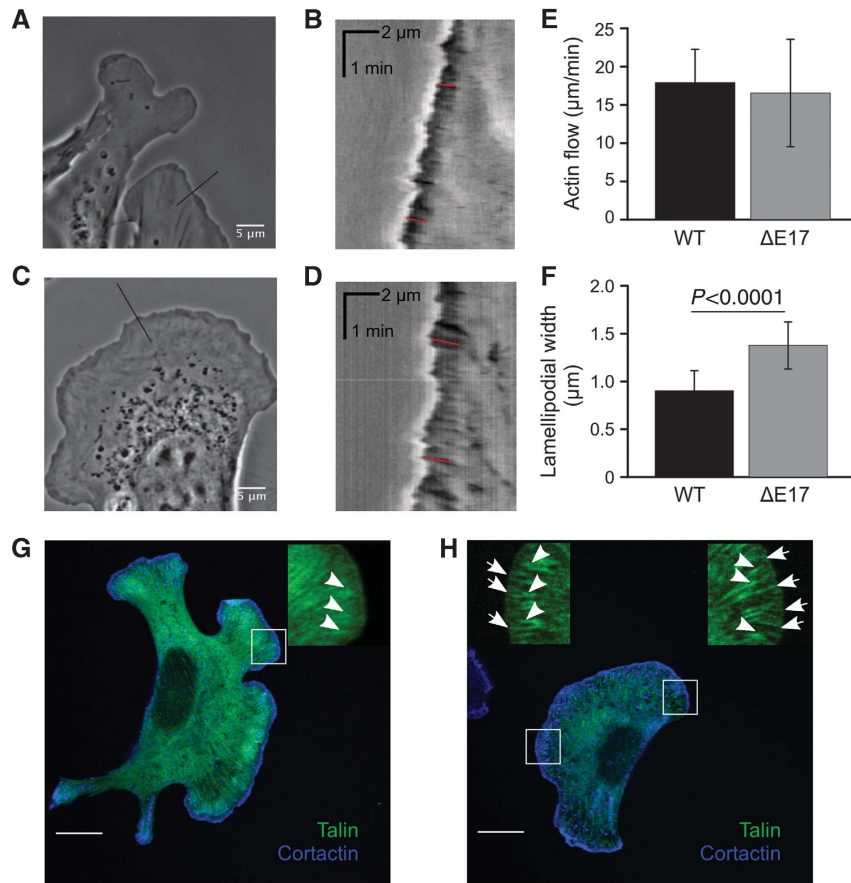


Figure 6 Enhanced phase contrast and fluorescence microscopy reveals an adhesion-actin coupling defect in PIPKI γ Δ E17 cells. (A) A single frame from a time-lapse series of WT cells. The black line marks the region from where a kymograph was generated. (B) The kymograph obtained from the wild-type cell depicted in (A). Red lines are examples of regions used to measure the distance and angle of the dark bands corresponding to retrograde actin flow. (C) A single frame from a time-lapse series of Δ E17 cells, showing the region from which the kymograph was derived (black line). (D) The kymograph obtained from the cell depicted in (C). Red lines are example regions used to calculate the length and angle of bands resulting from retrograde actin flow. (E, F) Lengths and angles of 50 actin flow lines from 9 cells of each genotype were used to calculate the rate of retrograde actin flow (E) and depth of penetration of the fast actin flow (defined as lamellipodial width) (F). Plots are mean \pm s.d. (G, H) GFP-talin-expressing WT (G) and Δ E17 cells (H) were immunostained for cortactin (blue) and localization of talin (green) relative to the lamellipodium was examined. Arrowheads denote adhesions that terminate at the lamella-lamellipodium border. Arrows in (H) highlight regions where the GFP-talin signal overlaps with the lamellipodium in Δ E17 cells.

PtdIns(4,5)P₂ at this location. We find that this specific pool of PtdIns(4,5)P₂ regulates the rate of talin recruitment into FAs. Although talin binds to PtdIns(4,5)P₂ at several locations within the FERM domain (Goksoy *et al*, 2008; Anthis *et al*, 2009; Saltel *et al*, 2009; Goult *et al*, 2010) mutational analysis shows that an interaction between PtdIns(4,5)P₂ and the talin F2 subdomain is responsible for mediating the recruitment of talin to adhesions. Preventing the autoinhibitory conformation by mutating residues important for the talin head-tail interaction did not normalize talin recruitment in Δ E17 cells. Therefore, the reduced recruitment rate does not result from a failure to activate talin. Abnormal recruitment of talin in Δ E17 cells has two consequences. First, the early formation of integrin-ligand bonds is impaired, leading to a reduced rate of initial cell attachment to FN-coated surfaces. Second, the transduction of force through integrins to the environment is reduced as a result of abnormal coupling of integrins to the actin cytoskeleton.

The earliest detectable consequence of impaired PtdIns(4,5)P₂ synthesis in FAs is a reduced rate of cell attachment. Our AFM experiments revealed a profound

delay in integrin-mediated attachment to a FN-coated surface in Δ E17 cells, which is reflected in the reduced adhesion of Δ E17 cells measured by a plate-and-wash assay. Since this assay measures the proportion of cells that adhere, but not how strongly they adhere (Boettiger and Wehrle-Haller, 2010), we also determined the rate of bond formation using spinning disc analysis. These experiments indicate that adherent Δ E17 cells accumulate integrin-ligand bonds at the same rate as WT cells. This observation contrasts with the reduced rate of talin recruitment in Δ E17 cells. Since talin binding to β -integrin tails has been described as an essential step in integrin activation (Tadokoro *et al*, 2003; Simonson *et al*, 2006; Wegener *et al*, 2007; Bouaouina *et al*, 2008) a similar reduction in the rate of bond formation ought to be expected, but it is not observed. Our data suggest that talin has an important role in initial cell matrix interactions but once a cell becomes adherent it does not contribute to additional integrin-ligand bonds. Extending this argument further, it may be postulated that talin facilitates a functional interaction between integrins and FN but is not essential for it to occur. Studies showing that depletion of both talin isoforms does

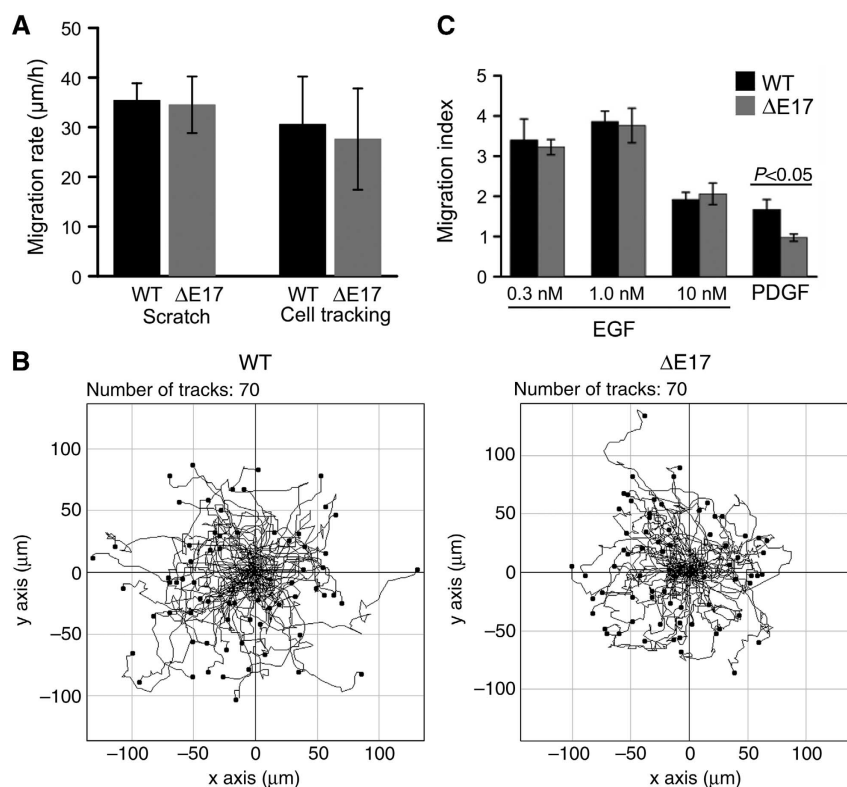


Figure 7 Migration analysis of wild-type and $\Delta E17$ cells. **(A)** Calculated migration speeds from the closure of a wounded cell monolayer (Scratch; mean \pm s.d. from four scratches for each genotype) or the manual tracking of sparsely seeded cells (mean \pm s.d. of 70 cells for each genotype). **(B)** Individual tracks of all cells from the manual tracking assay, plotted using the chemotaxis and migration plugin for ImageJ (Ibidi, Martinsried, DE). **(C)** Migration towards an EGF or PDGF gradient using a modified Boyden chamber transwell assay, using the indicated concentrations of EGF or 25 ng/ml PDGF. The migration index is the fold increase of migration across the filter in response to growth factor compared with 1% BSA. Data are mean \pm s.e.m. of three experiments.

not completely block adhesion or initial spreading in fibroblasts (Zhang *et al*, 2008), and does not impair the binding of $\beta 1$ -integrin to FN-coated beads (Roca-Cusachs *et al*, 2009) support this assertion.

The recruitment of kindlin 2 into adhesions was not affected by the absence of FA-localized PtdIns(4,5) P_2 synthesis. Therefore, PtdIns(4,5) P_2 binding does not serve as the rate-limiting step for kindlin 2 recruitment. It remains unknown whether PtdIns(4,5) P_2 is a true physiologic ligand for the kindlin 2 PH domain, but recent work suggests that it may bind PtdIns(3,4,5) P_3 most strongly (Qu *et al*, 2011). Our vesicle sedimentation assay demonstrates that kindlin 2 can bind anionic phospholipid vesicles rather non-specifically but in a cellular context kindlin 2 would encounter a broad choice of phosphoinositides to bind, and an array of competitors for lipid binding. Lipid signals may still influence kindlin 2 dynamics at the FA, but our study rules out PIPK1 γ_2 as the relevant lipid kinase.

The incorporation rate for kindlin 2 was higher than for talin (0.317 ± 0.037 /min for kindlin versus 0.233 ± 0.018 /min for talin), which may reflect the complexity of the interactions necessary for recruitment. Whereas kindlin 2 interacts with membrane distal sequences on the β -integrin tail and does not appear to require an interaction with lipids for assembly into FAs (Montañez *et al*, 2008; Qu *et al*, 2011) talin binds to β -integrin membrane distal sequences as well as to membrane proximal sequences which may be in close proximity with the α -integrin tail (Garcia-Alvarez *et al*, 2003; Wegener *et al*, 2007; Anthis *et al*, 2009). Furthermore,

interactions with the plasma membrane properly orient the talin head for productive binding to the membrane proximal sequences (Anthis *et al*, 2009; Kalli *et al*, 2010). Each of these interactions may represent a distinct binding step that together give rise to a lower rate of incorporation compared with FA components that have simpler modes of interaction. The higher kindlin 2 incorporation rate also suggests that kindlin assembles onto integrins before talin, but this has not been formally tested.

The coalescence of kindlin 2 into distinct adhesion structures visible by TIRF indicates that kindlin-integrin clusters could still form. By selectively slowing the incorporation of talin into adhesions in $\Delta E17$ cells, we have apparently uncoupled talin recruitment from integrin clustering. These data suggest that talin does not initiate integrin clustering, but it may stabilize clusters once they have formed. Depletion of both talin isoforms results in the absence of clustered integrins (Zhang *et al*, 2008) and disruption of talin-integrin binding destabilizes integrin clusters (Saltel *et al*, 2009), implying that talin is essential for the maintenance of these structures. We propose that talin achieves this by mediating the interaction between integrins and the cytoskeleton, thereby force coupling integrin to actin-myosin to maintain tension and to stabilize the integrin-FN bond.

Several lines of evidence also point to a force coupling defect in the absence of FA-localized PtdIns(4,5) P_2 synthesis. First, $\beta 1$ -integrin crosslinking to extracellular ligand is reduced in $\Delta E17$ cells, similar to what is observed when cells are treated with pharmacological inhibitors of myosin

function (Friedland *et al*, 2009). Second, the reduced Paxillin-positive area and adhesion length in Δ E17 cells support a force coupling defect as adhesion growth and elongation are regulated by the application of mechanical force to these structures (Balaban *et al*, 2001; Bershadsky *et al*, 2006). Third, Δ E17 cells are impaired in their ability to contract collagen gels despite a normal level of MLC phosphorylation. Fourth, direct measurement of force using traction force microscopy demonstrates that Δ E17 cells are deficient in force generation. Fifth, direct visualization of actin flow and indirect immunofluorescence assays revealed wider lamellipodia in Δ E17 cells that contain underlying talin-rich adhesion structures. Careful analysis has shown that the rate of lamellipodial actin flow is abruptly slowed over peripheral FAs, consistent with a model whereby integrin-associated actin-binding proteins capture fast moving actin filaments (Alexandrova *et al*, 2008; Gardel *et al*, 2008; Shemesh *et al*, 2009). According to our data, it is this capture step that is regulated by the local production of PtdIns(4,5)P₂ at FAs. Lamellipodial actin may be captured directly by talin (Hemmings *et al*, 1996; Lee *et al*, 2004; Gingras *et al*, 2008, 2010), or by talin-bound vinculin (Humphries *et al*, 2007), thus enabling a linkage between actin and integrins. The retarded recruitment of talin and vinculin in Δ E17 cells leads to a linkage that is slower to establish. A similar defect in coupling the cytoskeleton to the membrane has been reported in PIPKI γ -null megakaryocytes (Wang *et al*, 2008).

A force coupling defect manifested most strongly in gel contraction assays, but did not appear to play any role in non-directional cell migration or directed migration into a wound. In these assays, cells were adherent and spread for several days in the case of the scratch assay and the single-cell tracking assay also selected for adherent, spread cells. These data are consistent with reports that establish human PIPKI α (PIPKI β in mice), and not PIPKI γ , as an important mediator of cell migration through activating the small Rho GTPase Rac at lamellipodia, which in turn stimulates N-WASP-dependent actin polymerization (Mao *et al*, 2009; Chao *et al*, 2010). Under conditions where cells are already adherent and spread, PIPKI α -mediated PtdIns(4,5)P₂ synthesis at the lamellipodium may overcome the deficiency arising from loss of PIPKI γ _i2 to allow remodelling of adhesions at the leading edge and permit cell migration. As most of the defects observed as a result of impaired FA-PtdIns(4,5)P₂ synthesis occur at pre-steady-state conditions, and cell migration can be considered a rearrangement of the steady state, FA-localized PtdIns(4,5)P₂ synthesis may be most important under pre-steady-state conditions where diffusion of bulk PtdIns(4,5)P₂ is restricted or insufficient for the needs of the cell. Indeed, steady-state phenomena such as spreading area and adhesion area following prolonged incubation, or turnover of talin in mature FAs are not affected in Δ E17 cells (Figure 4D and unpublished data).

Chemotactic migration of Δ E17 fibroblasts towards a PDGF gradient was abolished, but migration towards EGF was not impaired. This contrasts with data showing that PIPKI γ _i2 is required for migration of HeLa cells towards EGF and hepatocyte growth factor (Sun *et al*, 2007). In these cells, PIPKI γ _i2 is required to assemble talin into FAs in the direction of the GF gradient; here, we demonstrate that talin recruitment is a general function of PIPKI γ _i2 that also occurs in the absence of GFs. Our finding that migration defects

arising from PIPKI γ _i2 deficiency depend on which GF is used as chemoattractant suggests that PIPKI γ _i2 may have an additional function downstream of GF signalling.

Significantly, the delay in integrin–ligand bond formation and failure to establish efficient force coupling are not corrected on a similar time scale. This suggests that the two functions of talin studied here show differential sensitivity to PtdIns(4,5)P₂, with force transduction being more sensitive to FA-localized PtdIns(4,5)P₂ synthesis. One intriguing possibility, suggested by the AFM data, is that β 1-integrin and β 3-integrin functions have different sensitivities to PtdIns(4,5)P₂ generated by PIPKI γ _i2. By using specific inhibitors, we could show that β 1-mediated binding is strongly influenced by PIPKI γ _i2, whereas β 3-mediated binding is insensitive to the absence of PIPKI γ _i2. Magnetic tweezer experiments have shown that while both β 1- and β 3-integrins can bind to FN-coated beads, only β 1-integrin mediates adhesion strength (Roca-Cusachs *et al*, 2009). The mechanism underlying different PtdIns(4,5)P₂ requirements for β 1- and β 3-integrin function is not known, but may also involve talin. Whereas the talin F3 domain is sufficient to activate β 3-integrin, β 1 additionally requires the F0/F1 domains (Bouaouina *et al*, 2008). An interaction between PtdIns(4,5)P₂ and sequences within the F1 domain may assist in aligning this part of the talin head with the membrane (Goult *et al*, 2010) and this orientation of the talin head may be important to facilitate force coupling by α 5 β 1-integrin. Future work will be heavily focused on deciphering the differences between β 1- and β 3-integrins and their requirement for localized PtdIns(4,5)P₂ production.

Alternatively, there may be additional PtdIns(4,5)P₂-sensitive structural interactions that depend on FA-localized PtdIns(4,5)P₂ synthesis that have not been examined here. Although the vinculin–talin interaction is critical for the induction of agonist-induced contraction of tracheal smooth muscle cells (Huang *et al*, 2010), vinculin function is unlikely to be impaired in our system as PtdIns(4,5)P₂ has been reported to inhibit rather than to promote actin binding (Steimle *et al*, 1999). An integrin–actin interaction via tensin may be perturbed, since tensin possesses PtdIns(4,5)P₂ binding activity (Leone *et al*, 2008), but the functional significance of phosphoinositide binding and a role for tensin in force coupling remain undefined. PtdIns(4,5)P₂ facilitates oligomerization of the heparin sulphate proteoglycan syndecan-4, which is also found in FAs (Woods and Couchman, 1994; Lee *et al*, 1998). Oligomerization of syndecan-4 is required for an interaction with the actin crosslinker α -actinin (Choi *et al*, 2008) but while syndecan-4 is well known to induce cytoskeleton reorganization (Couchman, 2010), a direct role in force transduction has not been reported.

Clearly, the role of PtdIns(4,5)P₂ in regulating FA dynamics is complex. By generating cell lines that are deficient in FA-localized PtdIns(4,5)P₂ synthesis we now have an important tool by which we can begin to address the importance of local, transient changes in PtdIns(4,5)P₂ concentration in a specific cellular process.

Materials and methods

Generation of a PIPKI γ _i2 knockout mouse and cell lines

A 495-bp DNA fragment surrounding PIPKI γ exon 17 was used to screen a PAC library. The PIPKI γ Δ E17 construct consisted of a

6.5-kb 5' arm followed by a 5' loxP site, exon 17, a neomycin cassette flanked by frt sites, a 3' loxP site and a 2.2-kb 3' arm. This construct was electroporated into 129 ES cells and 360 clones were isolated; 17 clones underwent homologous recombination. Two clones were chosen to derive PIPK1 γ Δ E17 mice.

To obtain Δ E17 fibroblasts, a kidney was removed from a 4-week-old PIPK1 γ Δ E17 fl/fl mouse and cells were obtained by macerating the kidney and digesting with 2 mg/ml collagenase for 30 min. Fibroblasts grew out of the culture within 1 week. Cells were immortalized by stable transduction with polyoma large T antigen and immortal lines were cloned. One line was chosen as the parental line, and the PIPK1 γ talin-binding sequence was deleted by transient transfection with an adenovirus encoding cre recombinase. Δ E17 lines were cloned and compared with the parental line in all experiments.

FA isolation and in vitro kinase assay

The cell binding fragment of FN (FNIII7-10; a gift from HP Erickson) was covalently coupled to Tosyl activated Dynabeads (Invitrogen) according to the manufacturer's directions. In all, 1×10^6 fibroblasts were incubated with 2×10^7 beads in DMEM + 1% BSA for 30 min at 37°C with end-over-end rotation. Beads were washed twice with DMEM + protease inhibitors (Roche) + phosphatase inhibitors (Sigma) and while magnetically restrained were sonicated at 15% power for 3×3 s pulses with a tip sonicator. Beads were passed $20 \times$ through a Dounce homogenizer and washed $5 \times$ with DMEM + phosphatase inhibitors. Washed beads were incubated with RIPA buffer and protein concentration was determined by BCA assay (Pierce).

Lipid kinase assays were performed as described (Dunlop and Muggli, 2000) using 1 μ g of protein in the presence or absence of 100 nM wortmannin and sonicated lipid solutions of 350 μ M phosphatidylserine, 500 μ M PI(4)P and 100 μ M phosphatidic acid.

TIRF-based incorporation assays

Cells were transiently transfected with plasmids encoding GFP-tagged proteins and analysed 24 h post-transfection. Cells were trypsinized and replated onto 5 μ g/ml FN-coated glass-bottom dishes and allowed to adhere for at least 1 h before analysis. Prior to analysis, media was exchanged for fluorescence microscopy buffer (10 mM HEPES-NaOH, 150 mM NaCl, 1 mM MgCl₂, 2 mM CaCl₂, 3 mM KCl and 22 mM glucose, pH 7.4) and plates were transferred to a heated stage of a Zeiss Axiovert 200 M fitted with a Coolsnap HQ camera and controlled by Metamorph software (Visitron Systems). 488 nm TIRF lasers were used to excite GFP. Images were collected every 5 s for 15 min. Calculation of incorporation rates from time-lapse series were determined as described (Franco *et al*, 2004).

Immunofluorescence assays

To examine coincidence of talin and paxillin in spreading cells, GFP-talin-expressing cells were plated onto 5 μ g/ml FN-coated coverslips for the indicated time periods, fixed with 4% paraformaldehyde (PFA) at 37°C and probed with a mouse anti-paxillin antibody followed by anti-mouse Cy3. For calculation of adhesion area and morphology of FAs, cells were prepared as above and probed with a mouse anti-paxillin antibody followed by anti-mouse Cy3 and Alexa 488-conjugated phalloidin. Images were collected with a Leica SP2 confocal microscope at $\times 100$ magnification and a digital zoom of 1.95. FA length was calculated by linear region selection in ImageJ. To examine coincidence of talin-rich adhesions with the lamellipodium, cells were transfected with GFP-talin and analysed 24 h post-transfection. Cells were trypsinized and transferred to 5 μ g/ml FN-coated coverslips for 2 h, fixed with 2% PFA for 15 min at 37°C and stained with a mouse anti-cortactin antibody and anti-mouse Alexa 647 secondary antibody. Images were taken sequentially with a Leica SP2 confocal microscope at $\times 100$ magnification and a digital zoom of 2.00, and merged.

Atomic force microscopy

AFM measurements were taken with a CellHesion 200 atomic force microscope (JPK Instruments). Cantilevers were calibrated using a thermal noise method provided by the JPK CellHesion 200 control software V.3.3, and force curves were analysed using JPK Image Processing software. Tipless silicon cantilevers (Arrow-TL1-50; Nanoworld) were coated with concanavalin A according to an established protocol (Franz *et al*, 2007) and used within 3 days.

Glass-bottom dishes were prepared with a drop of 2 μ g/ml FN and blocked with 1% BSA. Cells were trypsinized, resuspended in assay buffer (10 mM HEPES-NaOH, 150 mM NaCl, 1 mM MgCl₂, 2 mM CaCl₂, 3 mM KCl and 22 mM glucose, pH 7.4 containing the appropriate inhibitors, if applicable), and sparsely added to the dish. The plate was maintained at 37°C throughout the experiment with a heated stage. Individual cells were selected from a region of the dish containing no FN, and attached to the tip of a cantilever using visual guidance of a Zeiss Axiovert 200 M fitted with a $\times 20$ objective. Cells were allowed to attach to the cantilever, fully retracted from the surface for 5 min before force measurements were taken. During force measurement runs, cells approached a FN-coated region of the dish at 5 μ m/s and were brought into contact for the indicated times with a force of 200 pN, prior to retraction from the dish at 5 μ m/s. Cells were allowed to rest in the fully retracted position for 20 s between repeat measurements on adjacent FN-coated regions. Where indicated, experiments were performed in the presence of 0.2 mM linear RGD peptide (GRGDNP; Biomol), α 5 β 1 blocking antibody (MAB2575, Millipore) or 100 nM cilengitide (Horst Kessler, LMU, Munich).

Spinning disc assay

The spinning disc adhesion assay was performed as described (Boettiger, 2007). Briefly, 1×10^5 cells were plated onto FN- or VN-coated coverslips for the indicated times, before being affixed to the spinning disc apparatus and spun at 6000 r.p.m. in Dulbecco's PBS for 5 min. Coverslips were fixed in 2% PFA and stained with DAPI for automated counting using the $\times 10$ objective of a Zeiss Axiovert 200 M controlled by Metamorph software (version 7.7.0.0). Images were taken at defined positions of the coverslip, a threshold was applied and detected nuclei were assigned X and Y coordinates, which were recorded in an Excel file. Excel files were imported into Sigmaplot and data were graphed and fit to the equation $f = 1/(1 + \exp(b(\tau - c)))$, where $c = \tau_{50}$, the mean shear stress for cell detachment.

Integrin crosslinking assay

Cells were starved overnight, trypsinized and resuspended in Dulbecco's PBS + 2 mM glucose. In all, 1×10^6 cells were transferred to 6 cm dishes coated with 5 μ g/ml FN for the indicated times. Cells were incubated with 1 mM DTSSP (Thermo Scientific) at 4°C for 15 min, quenched with 50 mM Tris-Cl, pH 7.4 for 15 min and extracted with 20 mM Tris pH 7.4 + 0.1% SDS, 10 μ g/ml leupeptin, 10 μ g/ml aprotinin, and 1 mM PMSF. Plates were thoroughly washed with 20 mM Tris-Cl, pH 8.5 and crosslinks were broken by incubating plates with 20 mM Tris-Cl, pH 8.5, 25 mM DTT, 0.1% SDS for 1 h at 37°C. Crosslinked fractions were concentrated on Amicon Ultracel-30K filter units (Millipore) and loaded alongside 2% total extracted protein on 8% SDS-PAGE gels for analysis. Western blot images were collected using an LAS-4000 (Fujifilm) and band intensities were measured using ImageJ. Curves were fit in Sigmaplot to the first order reaction $y = a(1 - \exp(-bx))$.

Live-cell actin dynamics

Visualization of actin flow in living cells plated onto glass-bottom dishes coated with 5 μ g/ml FN for 2 h was performed on image series collected every 2 s for 5 min in a live-cell imaging chamber using the 100×1.6 objective of a Zeiss Axiovert 200 M controlled by Metamorph using the enhanced phase contrast technique (Verkhovsky *et al*, 2003). Kymographs were generated in ImageJ and straight-line selections were used to calculate actin flow and lamellipodial width.

Traction force microscopy

Gels (6.1% acrylamide/0.24% bisacrylamide) for traction experiments were cast on non-electrostatic silane-coated coverslips according to the procedure described by Pelham and Wang (1997). The Young's modulus of the gels was 12.8 kPa. Yellow-green fluorescent 0.5 mm carboxylated beads (Invitrogen) were suspended in the gels and centrifuged at 300 g towards the gel surface during polymerization at 4°C. These beads served as markers for gel deformations. The surface of the gel was activated with sulfo-SANPAH (Pierce Biotechnology, Rockford, IL) and coated with 50 mg/ml FN (Roche). Cells were seeded on top of the coated polyacrylamide gels and were cultured for 1 h to let them completely adhere. Cell tractions were computed from an unconstrained deconvolution of the gel surface displacement field

measured before and after cell detachment with 8 mM Cytochalasin D and Trypsin/EDTA (0.25/0.02%) in PBS (Butler *et al*, 2002). During the measurements, the cells were maintained at 37°C in humidified atmosphere containing 5% CO₂. Gel deformations were estimated using a Fourier-based difference-with-interpolation image analysis (Metzner *et al*, 2007). To characterize the contractile forces of each cell, the elastic strain energy stored in the polyacrylamide gel due to cell tractions was calculated as the product of local tractions and deformations, integrated over the spreading area of the cells (Butler *et al*, 2002).

MLC phosphorylation

In all, 10 cm dishes of subconfluent cell monolayers were harvested by washing with PBS and incubating on ice with 800 μ l 10% TCA/10 mM DTT. Material was scraped into a tube, washed twice with diethyl ether and dried under vacuum. Cell pellets were solubilized at room temperature with saturating amounts of urea in 20 mM glycine/22 mM Tris-Cl, pH 8.6, 1 mM EDTA, 10 mM DTT and 5% glycerol. MLC was separated from phospho-MLC by glycerol-urea PAGE (Garcia *et al*, 1995; Mehta *et al*, 2002).

Data analysis and statistics

Analysis of microscopy images was carried out using 64-bit ImageJ 1.43 (<http://rsb.info.nih.gov/ij/>) with the MBF 'ImageJ for Microscopy' plugins (http://www.macbiophotonics.ca/downloads/MBF_ImageJ.zip). Image Stabilizer plugin (http://www.cs.cmu.edu/~kangli/code/Image_Stabilizer.html) and Chemotaxis and Migration Tool (http://www.ibidi.de/applications/ap_chemo.html) installed. Statistical significance was established using either

Mann-Whitney tests using the R statistical software package, or using Sigmaplot. Non-linear best-fit lines and constants derived from them were generated in Sigmaplot.

Supplementary data

Supplementary data are available at *The EMBO Journal* Online (<http://www.embojournal.org>).

Acknowledgements

This work was supported by a Marie Curie fellowship under the European Community 6th framework program to KRL, by NIH grants DK065123, DK075594, DK65123 and DK083187; AHA established investigator award and a Merit award from the Department of Veterans Affairs to RZ, and the DFG (SFB 863) and Max Planck Society to RF.

Author contributions: The overall study was conceived and supervised by RF. KRL designed, performed and analysed most experiments. ST made the targeting construct enabling the generation of the cell lines. NB performed and analysed the traction force experiments, under the supervision of BF. DB contributed the spinning disc technology and participated in analysing the results. KRL, RF, DB and RZ wrote the manuscript.

Conflict of interest

The authors declare that they have no conflict of interest.

References

- Alexandrova AY, Arnold K, Schaub S, Vasiliev JM, Meister J-J, Bershadsky AD, Verkhovsky AB (2008) Comparative dynamics of retrograde actin flow and focal adhesions: formation of nascent adhesions triggers transition from fast to slow flow. *PLoS One* **3**: e3234
- Anthis NJ, Wegener KL, Ye F, Kim C, Goult BT, Lowe ED, Vakonakis I, Bate N, Critchley DR, Ginsberg MH, Campbell ID (2009) The structure of an integrin/talin complex reveals the basis of inside-out signal transduction. *EMBO J* **28**: 3623–3632
- Baird SF, Ling K, Su X, Firestone AJ, Carbonara C, Anderson RA (2006) Type I γ phosphatidylinositol phosphate kinase directly interacts with AP2 and regulates endocytosis. *J Biol Chem* **281**: 20632–20642
- Balaban NQ, Schwarz US, Riveline D, Goichberg P, Tzur G, Sabanay I, Mahalu D, Safran S, Bershadsky A, Addadi L, Geiger B (2001) Force and focal adhesion assembly: a close relationship studied using elastic micropatterned substrates. *Nat Cell Biol* **3**: 466–472
- Barsukov IL, Prescott A, Bate N, Patel B, Floyd DN, Bhanji N, Bagshaw CR, Letinic K, Di Paolo G, De Camilli P, Roberts GCK, Critchley DR (2003) Phosphatidylinositol phosphate kinase type I γ and beta1-integrin cytoplasmic domain bind to the same region in the talin FERM domain. *J Biol Chem* **278**: 31202–31209
- Bershadsky AD, Ballestrem C, Carramusa L, Zilberman Y, Gilquin B, Khochbin S, Alexandrova AY, Verkhovsky AB, Shemesh T, Kozlov MM (2006) Assembly and mechanosensory function of focal adhesions: experiments and models. *Eur J Cell Biol* **85**: 165–173
- Boettiger D (2007) Quantitative measurements of integrin-mediated adhesion to extracellular matrix. *Methods Enzymol* **426**: 1–25
- Boettiger D, Wehrle-Haller B (2010) Integrin and glycocalyx mediated contributions to cell adhesion identified by single cell force spectroscopy. *J Phys Condens Matter* **22**: 194101
- Bouaouina M, Lad Y, Calderwood DA (2008) The N-terminal domains of talin cooperate with the phosphotyrosine binding-like domain to activate beta1 and beta3 integrins. *J Biol Chem* **283**: 6118–6125
- Butler JP, Tolić-Nørrelykke IM, Fabry B, Fredberg JJ (2002) Traction fields, moments, and strain energy that cells exert on their surroundings. *Am J Physiol Cell Physiol* **282**: C595–C605
- Chao W-T, Daquinag AC, Ashcroft F, Kunz J (2010) Type I PIPK- α regulates directed cell migration by modulating Rac1 plasma membrane targeting and activation. *J Cell Biol* **190**: 247–262
- Choi Y, Kim S, Lee J, Ko S-G, Lee W, Han I-O, Woods A, Oh E-S (2008) The oligomeric status of syndecan-4 regulates syndecan-4 interaction with alpha-actinin. *Eur J Cell Biol* **87**: 807–815
- Couchman JR (2010) Transmembrane signaling proteoglycans. *Annu Rev Cell Dev Biol* **26**: 89–114
- Critchley DR (2004) Cytoskeletal proteins talin and vinculin in integrin-mediated adhesion. *Biochem Soc Trans* **32**: 831–836
- de Pereda JM, Wegener KL, Santelli E, Bate N, Ginsberg MH, Critchley DR, Campbell ID, Liddington RC (2005) Structural basis for phosphatidylinositol phosphate kinase type I γ binding to talin at focal adhesions. *J Biol Chem* **280**: 8381–8386
- Di Paolo G, Moskowitz HS, Gipson K, Wenk MR, Voronov S, Obayashi M, Flavell R, Fitzsimonds RM, Ryan TA, De Camilli P (2004) Impaired PtdIns(4,5)P₂ synthesis in nerve terminals produces defects in synaptic vesicle trafficking. *Nature* **431**: 415–422
- Di Paolo G, Pellegrini L, Letinic K, Cestra G, Zoncu R, Voronov S, Chang S, Guo J, Wenk MR, De Camilli P (2002) Recruitment and regulation of phosphatidylinositol phosphate kinase type I γ by the FERM domain of talin. *Nature* **420**: 85–89
- Doan AT, Huttenlocher A (2007) RACK1 regulates Src activity and modulates paxillin dynamics during cell migration. *Exp Cell Res* **313**: 2667–2679
- Dunlop ME, Muggli EE (2000) Extracellular matrix components cooperate to activate phosphatidylinositol-4-phosphate 5-kinase. *Biochem Biophys Res Commun* **279**: 931–937
- Franco SJ, Rodgers MA, Perrin BJ, Han J, Bennin DA, Critchley DR, Huttenlocher A (2004) Calpain-mediated proteolysis of talin regulates adhesion dynamics. *Nat Cell Biol* **6**: 977–983
- Frank AO, Otto E, Mas-Moruno C, Schiller HB, Marinelli L, Cosconati S, Bochen A, Vossmeier D, Zahn G, Stragies R, Novellino E, Kessler H (2010) Conformational control of integrin-subtype selectivity in isoDGR peptide motifs: a biological switch. *Angew Chem Int Ed Engl* **49**: 9278–9281
- Franz CM, Taubenberger A, Puech P-H, Muller DJ (2007) Studying integrin-mediated cell adhesion at the single-molecule level using AFM force spectroscopy. *Sci STKE* **2007**: pl5
- Friedland JC, Lee MH, Boettiger D (2009) Mechanically activated integrin switch controls alpha5beta1 function. *Science* **323**: 642–644

- García AJ, Huber F, Boettiger D (1998) Force required to break alpha5beta1 integrin-fibronectin bonds in intact adherent cells is sensitive to integrin activation state. *J Biol Chem* **273**: 10988–10993
- García JG, Davis HW, Patterson CE (1995) Regulation of endothelial cell gap formation and barrier dysfunction: role of myosin light chain phosphorylation. *J Cell Physiol* **163**: 510–522
- García-Alvarez B, de Pereda JM, Calderwood DA, Ulmer TS, Critchley D, Campbell ID, Ginsberg MH, Liddington RC (2003) Structural determinants of integrin recognition by talin. *Mol Cell* **11**: 49–58
- Gardel ML, Sabass B, Ji L, Danuser G, Schwarz US, Waterman CM (2008) Traction stress in focal adhesions correlates biphasically with actin retrograde flow speed. *J Cell Biol* **183**: 999–1005
- Giannone G, Mège R-M, Thoumine O (2009) Multi-level molecular clutches in motile cell processes. *Trends Cell Biol* **19**: 475–486
- Gingras AR, Bate N, Goult BT, Hazelwood L, Canestrelli I, Grossmann JG, Liu H, Putz NSM, Roberts GCK, Volkmann N, Hanein D, Barsukov IL, Critchley DR (2008) The structure of the C-terminal actin-binding domain of talin. *EMBO J* **27**: 458–469
- Gingras AR, Bate N, Goult BT, Patel B, Kopp PM, Emsley J, Barsukov IL, Roberts GCK, Critchley DR (2010) Central region of talin has a unique fold that binds vinculin and actin. *J Biol Chem* **285**: 29577–29587
- Giudici M-L, Emson PC, Irvine RF (2004) A novel neuronal-specific splice variant of Type I phosphatidylinositol 4-phosphate 5-kinase isoform gamma. *Biochem J* **379**: 489–496
- Goksoy E, Ma Y-Q, Wang X, Kong X, Perera D, Plow EF, Qin J (2008) Structural basis for the autoinhibition of talin in regulating integrin activation. *Mol Cell* **31**: 124–133
- Goult BT, Bate N, Anthis NJ, Wegener KL, Gingras AR, Patel B, Barsukov IL, Campbell ID, Roberts GCK, Critchley DR (2009) The structure of an interdomain complex that regulates talin activity. *J Biol Chem* **284**: 15097–15106
- Goult BT, Bouaouina M, Elliott PR, Bate N, Patel B, Gingras AR, Grossmann JG, Roberts GCK, Calderwood DA, Critchley DR, Barsukov IL (2010) Structure of a double ubiquitin-like domain in the talin head: a role in integrin activation. *EMBO J* **29**: 1069–1080
- Hemmings L, Rees DJ, Ohanian V, Bolton SJ, Gilmore AP, Patel B, Priddle H, Trevithick JE, Hynes RO, Critchley DR (1996) Talin contains three actin-binding sites each of which is adjacent to a vinculin-binding site. *J Cell Sci* **109** (Pt 11): 2715–2726
- Hilgemann DW (2007) Local PIP(2) signals: when, where, and how? *Pflugers Arch* **455**: 55–67
- Huang Y, Zhang W, Gunst SJ (2010) Activation of vinculin induced by cholinergic stimulation regulates contraction of tracheal smooth muscle tissue. *J Biol Chem* **286**: 3630–3644
- Humphries JD, Wang P, Streuli C, Geiger B, Humphries MJ, Ballestrem C (2007) Vinculin controls focal adhesion formation by direct interactions with talin and actin. *J Cell Biol* **179**: 1043–1057
- Hynes RO (2002) Integrins: bidirectional, allosteric signaling machines. *Cell* **110**: 673–687
- Ishihara H, Shibasaki Y, Kizuki N, Katagiri H, Yazaki Y, Asano T, Oka Y (1996) Cloning of cDNAs encoding two isoforms of 68-kDa type I phosphatidylinositol-4-phosphate 5-kinase. *J Biol Chem* **271**: 23611–23614
- Ishihara H, Shibasaki Y, Kizuki N, Wada T, Yazaki Y, Asano T, Oka Y (1998) Type I phosphatidylinositol-4-phosphate 5-kinases. Cloning of the third isoform and deletion/substitution analysis of members of this novel lipid kinase family. *J Biol Chem* **273**: 8741–8748
- Kalli AC, Wegener KL, Goult BT, Anthis NJ, Campbell ID, Sansom MSP (2010) The structure of the talin/integrin complex at a lipid bilayer: an NMR and MD simulation study. *Structure* **18**: 1280–1288
- Kong F, García AJ, Mould AP, Humphries MJ, Zhu C (2009) Demonstration of catch bonds between an integrin and its ligand. *J Cell Biol* **185**: 1275–1284
- Lee D, Oh ES, Woods A, Couchman JR, Lee W (1998) Solution structure of a syndecan-4 cytoplasmic domain and its interaction with phosphatidylinositol 4,5-bisphosphate. *J Biol Chem* **273**: 13022–13029
- Lee H-S, Bellin RM, Walker DL, Patel B, Powers P, Liu H, Garcia-Alvarez B, de Pereda JM, Liddington RC, Volkmann N, Hanein D, Critchley DR, Robson RM (2004) Characterization of an actin-binding site within the talin FERM domain. *J Mol Biol* **343**: 771–784
- Legate KR, Fässler R (2009) Mechanisms that regulate adaptor binding to beta-integrin cytoplasmic tails. *J Cell Sci* **122**: 187–198
- Legate KR, Wickström SA, Fässler R (2009) Genetic and cell biological analysis of integrin outside-in signaling. *Genes Dev* **23**: 397–418
- Leone M, Yu EC, Liddington RC, Pasquale EB, Pellicchia M (2008) The PTB domain of tensin: NMR solution structure and phosphoinositides binding studies. *Biopolymers* **89**: 86–92
- Ling K, Bairstow SF, Carbonara C, Turbin DA, Huntsman DG, Anderson RA (2007) Type I gamma phosphatidylinositol phosphate kinase modulates adherens junction and E-cadherin trafficking via a direct interaction with mu 1B adaptin. *J Cell Biol* **176**: 343–353
- Ling K, Doughman RL, Firestone AJ, Bunce MW, Anderson RA (2002) Type I gamma phosphatidylinositol phosphate kinase targets and regulates focal adhesions. *Nature* **420**: 89–93
- Loijens JC, Anderson RA (1996) Type I phosphatidylinositol-4-phosphate 5-kinases are distinct members of this novel lipid kinase family. *J Biol Chem* **271**: 32937–32943
- Lokuta MA, Senetar MA, Bennin DA, Nuzzi PA, Chan KT, Ott VL, Huttenlocher A (2007) Type I gamma PIP kinase is a novel uropod component that regulates rear retraction during neutrophil chemotaxis. *Mol Biol Cell* **18**: 5069–5080
- Mao YS, Yamaga M, Zhu X, Wei Y, Sun H-Q, Wang J, Yun M, Wang Y, Di Paolo G, Bennett M, Mellman I, Abrams CS, De Camilli P, Lu CY, Yin HL (2009) Essential and unique roles of PIP5K-gamma and -alpha in Fc gamma receptor-mediated phagocytosis. *J Cell Biol* **184**: 281–296
- McLaughlin S, Murray D (2005) Plasma membrane phosphoinositide organization by protein electrostatics. *Nature* **438**: 605–611
- Mehta D, Tirupathi C, Sandoval R, Minshall RD, Holinstat M, Malik AB (2002) Modulatory role of focal adhesion kinase in regulating human pulmonary arterial endothelial barrier function. *J Physiol (Lond)* **539**: 779–789
- Metzner C, Raupach C, Zitterbart DP, Fabry B (2007) Simple model of cytoskeletal fluctuations. *Phys Rev E Stat Nonlin Soft Matter Phys* **76**: 021925
- Montañez E, Ussar S, Schifferer M, Bösl M, Zent R, Moser M, Fässler R (2008) Kindlin-2 controls bidirectional signaling of integrins. *Genes Dev* **22**: 1325–1330
- Moser M, Legate KR, Zent R, Fässler R (2009) The tail of integrins, talin, and kindlins. *Science* **324**: 895–899
- Palmer SM, Playford MP, Craig SW, Schaller MD, Campbell SL (2009) Lipid binding to the tail domain of vinculin: specificity and the role of the N and C termini. *J Biol Chem* **284**: 7223–7231
- Pelham Jr RJ, Wang YI (1997) Cell locomotion and focal adhesions are regulated by substrate flexibility. *Proc Natl Acad Sci USA* **94**: 13661–13665
- Qu H, Tu Y, Shi X, Larjava H, Saleem MA, Shattil SJ, Fukuda K, Qin J, Kretzler M, Wu C (2011) Kindlin-2 regulates podocyte adhesion and fibronectin matrix deposition through interactions with phosphoinositides and integrins. *J Cell Sci* **124**: 879–891
- Roca-Cusachs P, Gauthier NC, Del Rio A, Sheetz MP (2009) Clustering of alpha(5)beta(1) integrins determines adhesion strength whereas alpha(v)beta(3) and talin enable mechanotransduction. *Proc Natl Acad Sci USA* **106**: 16245–16250
- Saltel F, Mortier E, Hytönen VP, Jacquier M-C, Zimmermann P, Vogel V, Liu W, Wehrle-Haller B (2009) New PI(4,5)P2- and membrane proximal integrin-binding motifs in the talin head control beta3-integrin clustering. *J Cell Biol* **187**: 715–731
- Schill NJ, Anderson RA (2009) Two novel phosphatidylinositol-4-phosphate 5-kinase type I gamma splice variants expressed in human cells display distinctive cellular targeting. *Biochem J* **422**: 473–482
- Shemesh T, Verkhovsky AB, Svitkina TM, Bershadsky AD, Kozlov MM (2009) Role of focal adhesions and mechanical stresses in the formation and progression of the lamellipodium-lamellum interface [corrected]. *Biophys J* **97**: 1254–1264
- Shi Q, Boettiger D (2003) A novel mode for integrin-mediated signaling: tethering is required for phosphorylation of FAK Y397. *Mol Biol Cell* **14**: 4306–4315
- Simonson WTN, Franco SJ, Huttenlocher A (2006) Talin1 regulates TCR-mediated LFA-1 function. *J Immunol* **177**: 7707–7714
- Steimle PA, Hoffert JD, Adey NB, Craig SW (1999) Polyphosphoinositides inhibit the interaction of vinculin with actin filaments. *J Biol Chem* **274**: 18414–18420

- Sun Y, Ling K, Wagoner MP, Anderson RA (2007) Type I gamma phosphatidylinositol phosphate kinase is required for EGF-stimulated directional cell migration. *J Cell Biol* **178**: 297–308
- Tadokoro S, Shattil SJ, Eto K, Tai V, Liddington RC, De Pereda JM, Ginsberg MH, Calderwood DA (2003) Talin binding to integrin beta tails: a final common step in integrin activation. *Science* **302**: 103–106
- Vasudevan L, Jeromin A, Volpicelli-Daley L, De Camilli P, Holowka D, Baird B (2009) The beta- and gamma-isoforms of type I PIP5K regulate distinct stages of Ca²⁺ signaling in mast cells. *J Cell Sci* **122**: 2567–2574
- Verkhovskiy AB, Chaga OY, Schaub S, Svitkina TM, Meister J-J, Borisy GG (2003) Orientational order of the lamellipodial actin network as demonstrated in living motile cells. *Mol Biol Cell* **14**: 4667–4675
- Wang Y, Lian L, Golden JA, Morrissey EE, Abrams CS (2007) PIP5K1 gamma is required for cardiovascular and neuronal development. *Proc Natl Acad Sci USA* **104**: 11748–11753
- Wang Y, Litvinov RI, Chen X, Bach TL, Lian L, Petrich BG, Monkley SJ, Kanaho Y, Critchley DR, Sasaki T, Birnbaum MJ, Weisel JW, Hartwig J, Abrams CS (2008) Loss of PIP5K1 gamma, unlike other PIP5K1 isoforms, impairs the integrity of the membrane cytoskeleton in murine megakaryocytes. *J Clin Invest* **118**: 812–819
- Wang YJ, Li WH, Wang J, Xu K, Dong P, Luo X, Yin HL (2004) Critical role of PIP5K1{gamma}87 in InsP3-mediated Ca(2+) signaling. *J Cell Biol* **167**: 1005–1010
- Wegener KL, Partridge AW, Han J, Pickford AR, Liddington RC, Ginsberg MH, Campbell ID (2007) Structural basis of integrin activation by talin. *Cell* **128**: 171–182
- Wernimont SA, Legate KR, Simonson WTN, Fassler R, Huttenlocher A (2010) PIPKI gamma 90 negatively regulates LFA-1-mediated adhesion and activation in antigen-induced CD4+ T cells. *J Immunol* **185**: 4714–4723
- Woods A, Couchman JR (1994) Syndecan 4 heparan sulfate proteoglycan is a selectively enriched and widespread focal adhesion component. *Mol Biol Cell* **5**: 183–192
- Xu W, Wang P, Petri B, Zhang Y, Tang W, Sun L, Kress H, Mann T, Shi Y, Kubes P, Wu D (2010) Integrin-induced PIP5K1C kinase polarization regulates neutrophil polarization, directionality, and *in vivo* infiltration. *Immunity* **33**: 340–350
- Zaidel-Bar R, Itzkovitz S, Ma'ayan A, Iyengar R, Geiger B (2007) Functional atlas of the integrin adhesome. *Nat Cell Biol* **9**: 858–867
- Zhang X, Jiang G, Cai Y, Monkley SJ, Critchley DR, Sheetz MP (2008) Talin depletion reveals independence of initial cell spreading from integrin activation and traction. *Nat Cell Biol* **10**: 1062–1068